

## Supporting Information

### **Mottness collapse in monolayer 1T-TaSe<sub>2</sub> with persisting charge density wave order**

Kang Zhang<sup>1</sup>, Chen Si<sup>1,2\*</sup>, Chao-Sheng Lian<sup>3</sup>, Jian Zhou<sup>1</sup>, and Zhimei Sun<sup>1,2\*</sup>

<sup>1</sup> *School of Materials Science and Engineering, Beihang University, Beijing 100191, China*

<sup>2</sup> *Center for Integrated Computational Materials Engineering, International Research Institute for  
Multidisciplinary Science, Beihang University, Beijing 100191, China*

<sup>3</sup> *International Laboratory for Quantum Functional Materials of Henan, School of Physics and  
Microelectronics, Zhengzhou University, Zhengzhou 450001, China*

\*Emails: [sichen@buaa.edu.cn](mailto:sichen@buaa.edu.cn); [zmsun@buaa.edu.c](mailto:zmsun@buaa.edu.c)

## 1. Spin-polarized electronic structure in the CDW phase within the GGA + U method.

Fig. S1 shows the spin-polarized band structures calculated within the GGA+U method with the on-site effective  $U$  ranging from 1 to 4 eV. Similar to the spin-polarized GGA, under GGA+U, the flat band is also split into LHB and UHB, resulting in an insulating ground state, but the fundamental gap is larger than that in GGA and increases with  $U$ .

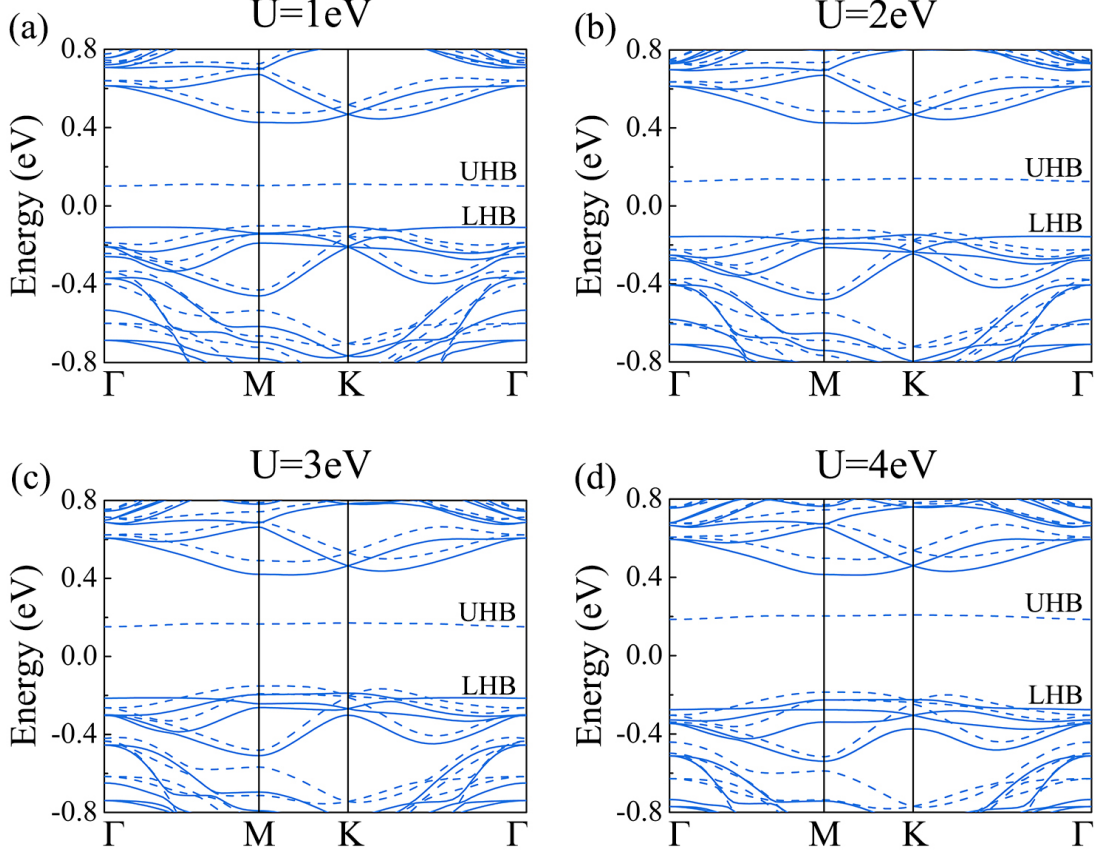


**Fig. S1** Spin-polarized electronic structures in the CDW phase within GGA + U. The solid and dashed lines represent the spin-up and spin-down channels, respectively.

## 2. Effects of spin orbit coupling (SOC) on the electronic structure of 1T-TaSe<sub>2</sub>.

Fig. S2 shows the band structures of 1T-TaSe<sub>2</sub> in the normal and the CDW phase calculated with and without SOC. For the undistorted normal phase, the main effects of SOC are lifting the band degeneracy at certain high-symmetry points. For the CDW phase, similar to the spin-polarized band structure, the band structure under SOC also shows an insulating gap with a slightly smaller size. Overall, SOC does not play an important role in the discussed physics and thus is neglected.

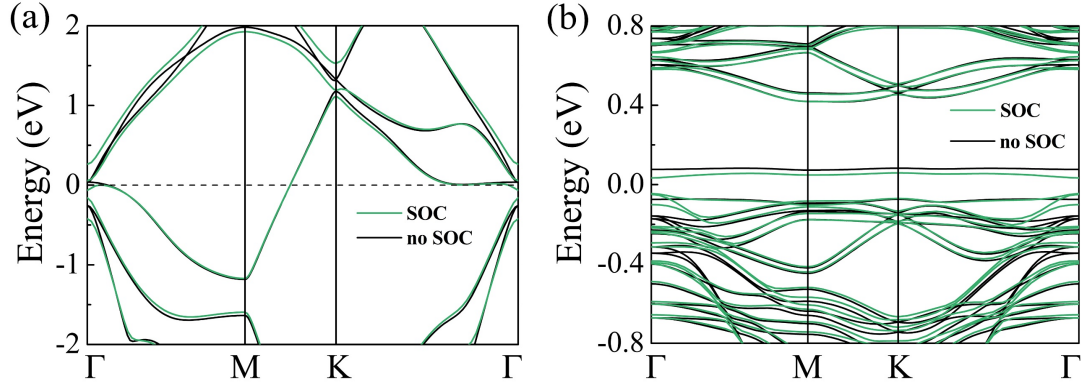


**Fig. S2** Electronic band structures of monolayer 1T-TaSe<sub>2</sub> in the undistorted normal phase (a) and CDW phase (b) with and without spin-orbit coupling (SOC). The band structure without SOC in (b) is calculated using spin-polarized GGA.

### 3. Theoretical method for applying biaxial strain

We applied biaxial in-plane strain by introducing homogenous biaxial expansion or compression in both x and y directions of the lattice, as shown in Fig. S3.

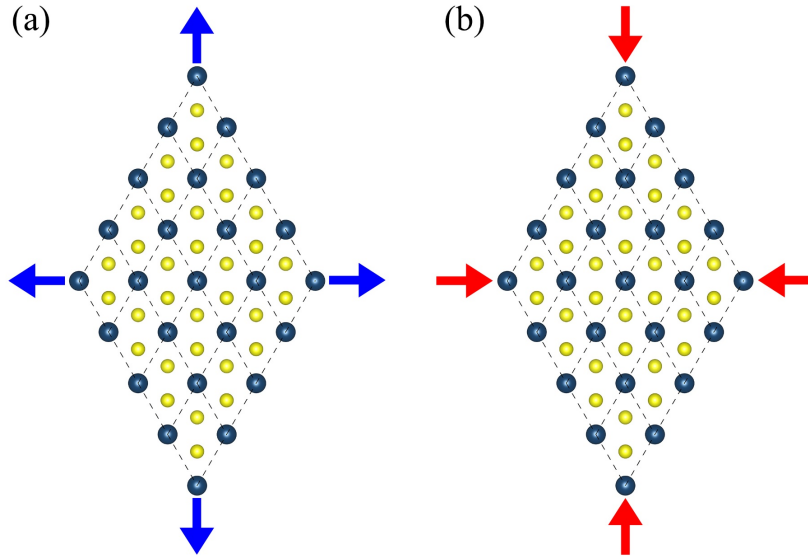


**Fig. S3** In-plane biaxial strain is applied by uniformly stretching (a) or compressing (b) the lattice along both the x and y directions. Blue and red arrows represent expansion and compression, respectively.

### 4. Band structures for the 1T-TaSe<sub>2</sub> CDW phase under different strains.

Fig. S4 summarizes the band structures of the CDW phase under strain ranging from -4% to 4%.

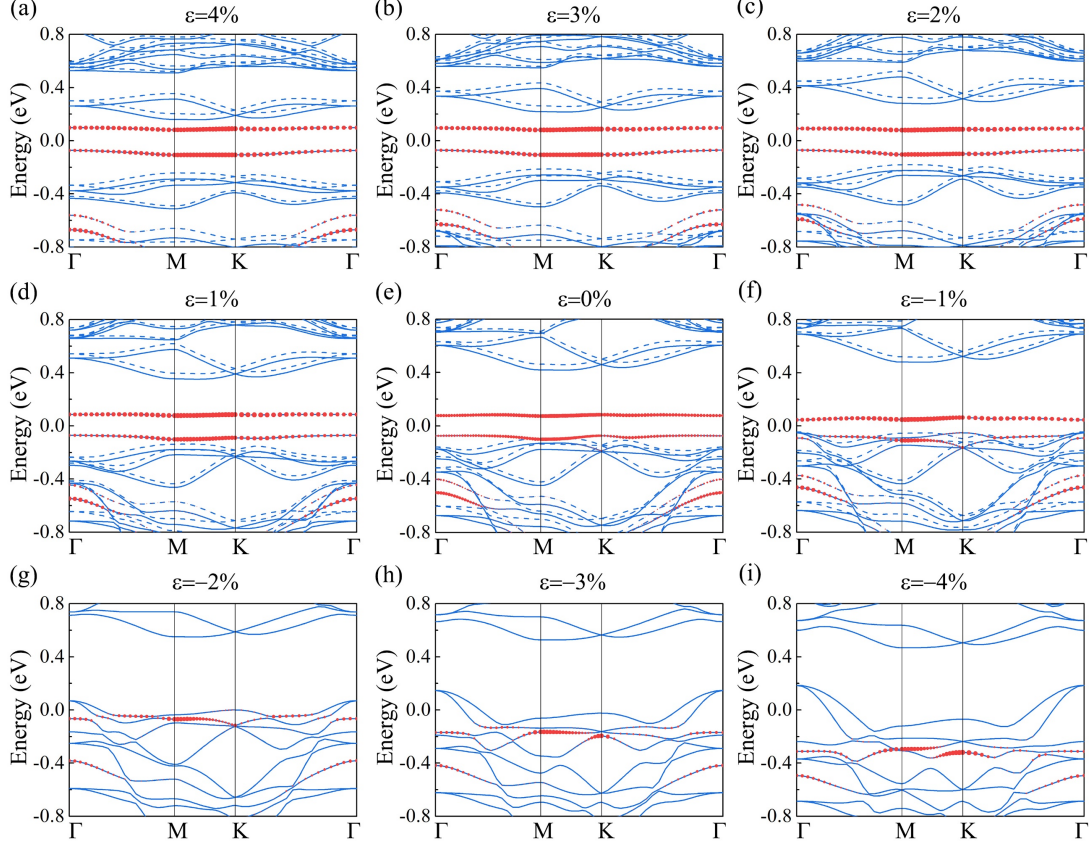


**Fig. S4** Band structures in the 1T-TaSe<sub>2</sub> CDW phase under the strain ranging from 4% to -4%. The red dots represent the weights of the center Ta  $d_z^2$  orbitals. Solid and dashed lines are the majority and minority spin bands, respectively.

## 5. The evolution of the CDW gap with strain.

The periodic CDW distortion will generally induce the opening of a CDW gap. To show the formation of the CDW gap, we have unfolded the nonmagnetic band structure of the CDW phase into the primitive Brillouin zone and made a direct comparison with the band structure of normal phase, as shown in Fig. S5(a) below and Fig. 2(c) in the manuscript. It is seen that the CDW distortion makes the bands crossing the Fermi level gapped, leading to the formation of a CDW gap of  $\sim 0.43$  eV. We further plot the unfolded band structures of the CDW phase under different strains in Fig. S5(b)-(e). It is clearly seen that the CDW gap is always present, although its size changes with the applied strain. As shown in Fig. S5(f), when the tensile strain increases from 0% to 4%, the CDW gap monotonously decreases from 0.43 eV to 0.17 eV. Under the compressive strain, the CDW gap firstly increases to 0.50 eV at -1% strain and then decreases as the strain increases. The variation of the CDW gap size should arise from the conspiracy of the changes of the CDW distortion amplitude and the CDW lattice constant. Note that the CDW gap and the Mott gap are two different physical quantities. The former directly comes from the CDW distortion, while the latter is dominated by the electronic correlation. Therefore, when the applied compressive strain is larger than a critical value, although the CDW distortion and the CDW gap persist, the Mottness collapses due to the weakening of the electronic localization.

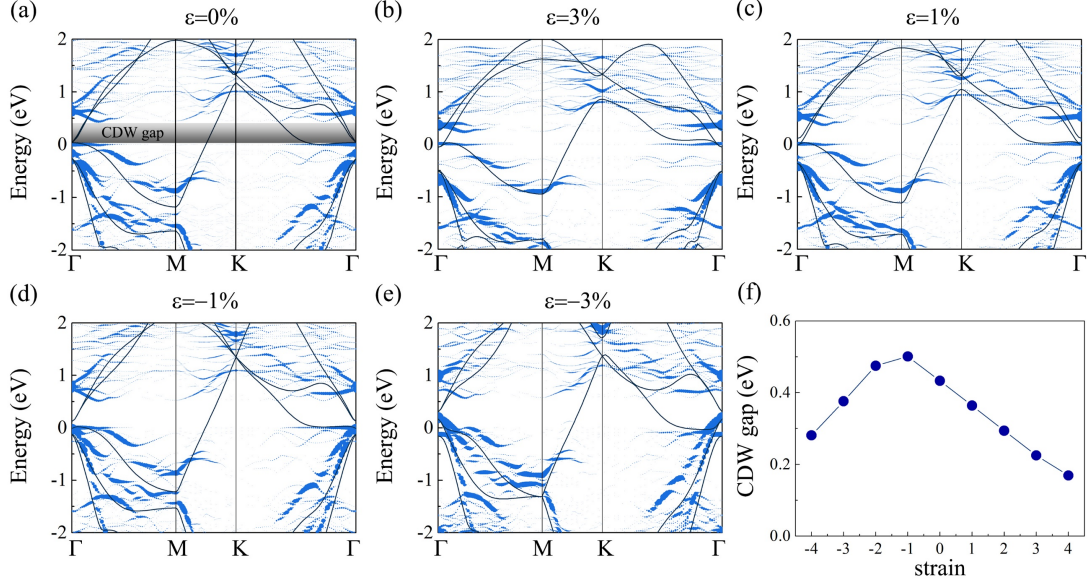


**Fig. S5** (a)-(e) Unfolded band structures of CDW phase into the primitive Brillouin zone under strains ( $\epsilon$ ) of 0%,  $\pm 1\%$  and  $\pm 3\%$ . (f) The CDW gap in 1T-TaSe<sub>2</sub> as the function of the biaxial strain.

## 6. Effects of charge doping on the CDW.

In this part, we considered the effects of charge doping on the CDW phase of monolayer 1T-TaSe<sub>2</sub>. First, we calculate the CDW formation energy  $\Delta E$  as a function of doping concentration, as shown in Fig. S6. Overall, within a typical doping concentration ranging from  $-10^{14}$  cm<sup>-2</sup> (hole doping) to  $10^{14}$  cm<sup>-2</sup> (electron doping), the CDW order is always maintained, although the absolute value of its formation energy ( $|\Delta E|$ ) decreases (increases) as the hole (electron) doping concentration increases.

Second, we show the evolution of the band structure of the CDW phase under charge doping (see Fig. S7). Without charge doping, the half-filled flat band in the gap between the valence and conduction bands is split into two bands labeled as LHB and UHB, respectively (LHB is filled by a spin-up electron, while UHB is empty), yielding a Mott-insulating ground state (Fig. S7(c)). When the CDW phase is doped by charge smaller than 1 electron (hole) per David-Star cluster, which corresponds to a doping concentration smaller than  $7.2 \times 10^{13}$  cm<sup>-2</sup>, the UHB (LHB) will become partially occupied (see Figs. S7(b) and S7(d)). In this case, the CDW phase becomes a doped Mott insulator. When no less than 1 electron (hole) per David-Star cluster are doped into the CDW structure, the original flat band will be fully occupied (empty) and no longer be split, as shown in Figs. S7(a) and 7(e), resulting in the collapse of the Mott phase.

Generally, at experiment the concentration of charge doping from the substrate is smaller than  $10^{13}$  cm<sup>-2</sup>. According to the above calculations, it is clearly seen that this small amount of charge doping will not lead to the CDW suppression and the Mottness collapse in monolayer TaSe<sub>2</sub>.

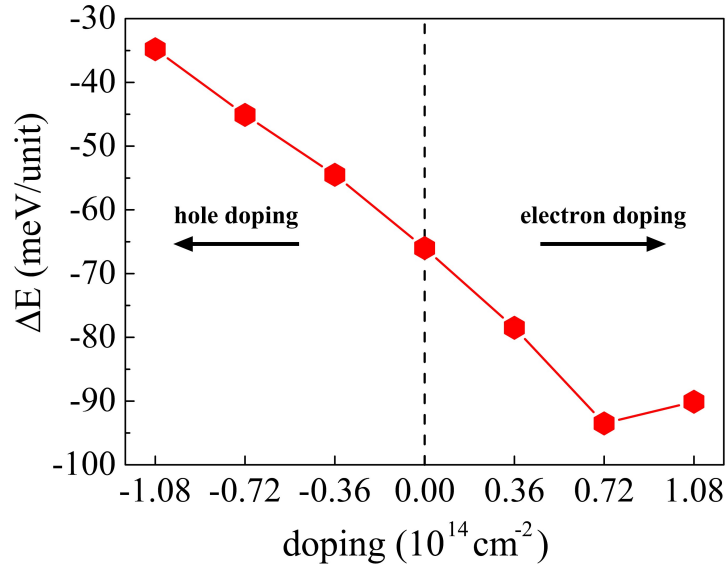


**Fig. S6** CDW formation energy  $\Delta E$  as a function of doping. The positive (negative) doping value represents electron (hole) doping.

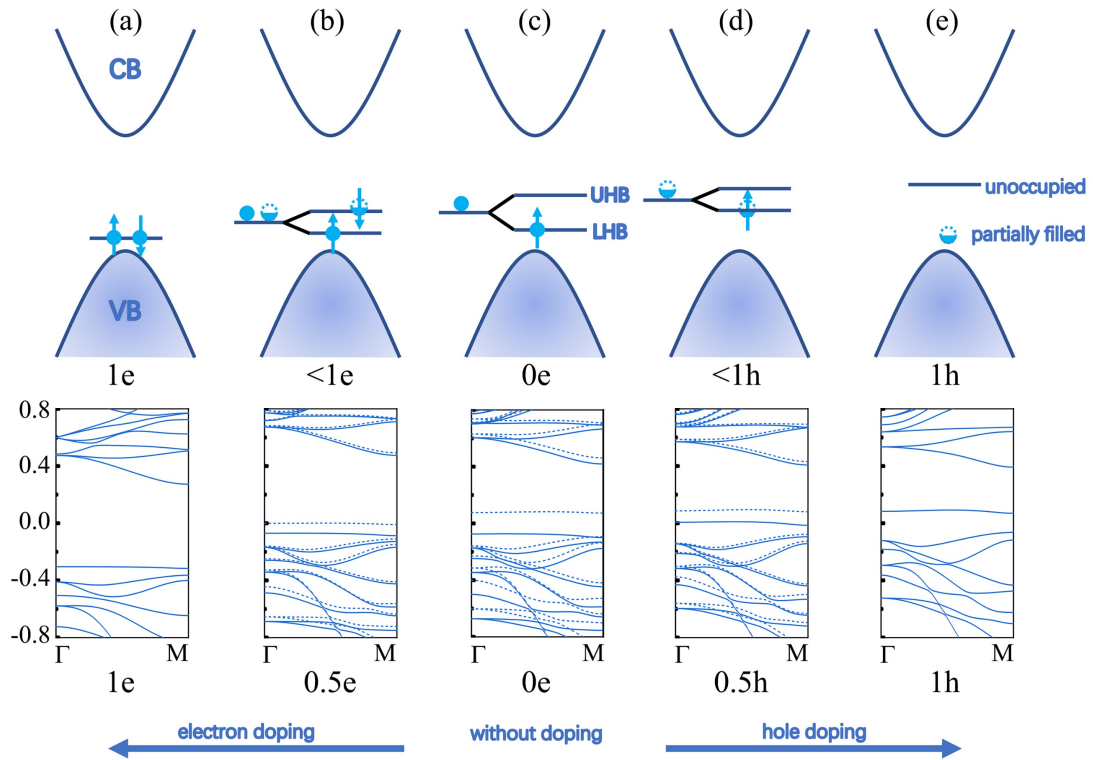


**Fig. S7** [Upper panels] The energy level schematic diagrams of the 1T-TaSe<sub>2</sub> CDW phase with doping of 1 electron (a), < 1 electron (b), zero electron (c), < 1 hole (d) and 1 hole (e) per David-Star cluster. [Bottom panels] Corresponding band structures calculated from first-principles, in good agreement with the energy level schematics.

## 7. Detailed data set of CDW phase with strain.

Table S1 shows the detailed data set which contains the lattice parameter, the CDW formation energy, the band gap and the total magnetic moment of the CDW phase as a function of the applied strain ranging from 4% to -4%.

**Table S1** Lattice parameter  $a$ , CDW formation energy  $\Delta E$ , band gap  $E_g$  and total magnetic moment  $M$  of the CDW phase under the biaxial strain ranging from 4% to -4%.

strain	4%	3%	2%	1%	0%	-1%	-2%	-3%	-4%
$a$ (Å)	13.146	13.019	12.893	12.766	12.640	11.882	12.387	12.261	12.134
$\Delta E$ (meV/TaSe <sub>2</sub> formula)	-69.98	-68.44	-67.35	-66.51	-66.02	-66.23	-68.59	-74.31	-79.73
$E_g$ (eV)	0.155	0.152	0.151	0.148	0.147	0.097	0	0	0
$M$ ( $\mu_B$ /star)	1	1	1	1	1	0.929	0	0	0

## 8. CDW formation energy under strain for different CDW periodicities.

In addition to the  $\sqrt{13} \times \sqrt{13}$  CDW order, we checked other CDW orders including  $3 \times 3$ ,  $4 \times 4$  and  $5 \times 5$ . Their formation energies are shown in Table S2. Under the external strain of 0%, +3% and -3%, it is clearly seen that the  $\sqrt{13} \times \sqrt{13}$  CDW order always has the largest energy gain.

**Table S2:** CDW formation energies (unit: meV/TaSe<sub>2</sub> formula) as a function of strain for different CDW periodicities.

strain periodicities	3%	0%	-3%
$\sqrt{13} \times \sqrt{13}$	-68.4	-66.0	-74.3
$3 \times 3$	-6.7	-3.1	2.3
$4 \times 4$	-14.2	-38.4	-7.9
$5 \times 5$	-3.3	-26.2	7.2